Journal of Power Sources 195 (2010) 3498–3503

Contents lists available at ScienceDirect

Journal of Power Sources

journal homepage: www.elsevier.com/locate/jpowsour

Short communication

Pt overgrowth on carbon supported PdFe seeds in the preparation of core–shell electrocatalysts for the oxygen reduction reaction

Wei Wang[a], Rongfang Wang[a,*], Shan Ji[b], Hanqing Feng[c], Hui Wang[a], Ziqiang Lei[a,**]

[a] Key Laboratory of Eco-Environment-Related Polymer Materials, Ministry of Education of China, Key Laboratory of Gansu Polymer Materials, College of Chemistry and Chemical Engineering, Northwest Normal University, Anning Road 967, Lanzhou 730070, China
[b] South African Institute for Advanced Materials Chemistry, University of the Western Cape, Cape Town, South Africa
[c] College of Life Science, Northwest Normal University, Lanzhou 730070, China

ARTICLE INFO

Article history:
Received 31 October 2009
Received in revised form 2 December 2009
Accepted 3 December 2009
Available online 29 December 2009

Keywords:
Electrocatalysts
Core–shell structure
Oxygen reduction reaction
Fuel cells

ABSTRACT

In this study, a novel core–shell structured Pd_3Fe@Pt/C electrocatalyst, which is based on Pt deposited onto carbon supported Pd_3Fe nanoparticles, is prepared for the oxygen reduction reaction (ORR) in proton exchange membrane fuel cells (PEMFCs). The carbon supported Pd_3Fe nanoparticles act as seeds to guide the growth of Pt. The formation of the core–shell structured Pd_3Fe@Pt/C is confirmed by transmission electron microscopy (TEM), X-ray diffraction (XRD) and electrochemical characterization. The higher surface area of the synthesized catalyst suggests that the utilization of Pt in the Pd_3Fe@Pt/C catalyst is higher than that in Pt/C. Furthermore, better electrocatalytic performance than that of Pt/C and Pd_3Fe/C catalyst is observed in the ORR which follows a four-electron path. Consequently, the results indicate that the Pd_3Fe@Pt/C catalyst could be used as a more economically viable alternative for the ORR of PEMFCs.

1. Introduction

Considerable attention has been paid to alternative energy sources in an attempt to relieve the pollution and energy crisis [1]. One of the promising fields of clean and sustainable power is low-temperature fuel cell technology, based on direct conversation of fuel into electricity. Despite considerable advances in recent years, many technical barriers still need to overcome in the development of electrocatalysts for widespread commercialization. Platinum-based catalysts are state-of-the-art materials for the oxygen reduction reaction (ORR) in low-temperature fuel cells [2]. The fuel cell operates at ambient conditions using platinum and platinum alloys for the conversation of fuel at the cathode side. However, high cost of platinum significantly increases the total price of fuel cell devices [3].

In an effort to improve catalyst activity and reduce the cost of the catalyst, many modified Pt-based catalysts have been synthesized for the fuel cells, such as Pt–Ti, Pt–Pd, Pt–Co, Pt–Cr, Pt–Mn, and Pt–Fe [4–7]. However, these modifications still require a relatively high Pt loading. Recently, reports also indicate that the activity of binary Pd–M alloys (M = Cr, Co, Fe, Ni, Ti) and ternary ones were comparable to, or slightly better than that of commercial Pt catalysts. These Pd–M catalysts have attracted considerable attention because they are comparatively cheap and have very high methanol tolerance, making them promising cathode materials for proton exchange membrane fuel cells (PEMFCs) [8,9].

Now, one of the main challenges to commercialization of fuel cell is to develop cheap and stable fuel cell catalysts for the ORR, in order to dramatically reduce the cost and increase the efficiency of the catalysts [10]. To further reduce the content of the noble metals used in PEMFCs, core–shell nanoparticles were investigated as possible catalyst candidates for oxygen reduction [11,12]. By properly selecting the core of catalysts, the activity of Pt shell can be enhanced through structural- and/or electronic-effects [13]. Recent research shows that core–shell catalysts, such as Fe@Pt, Co@Pt, Cu@Pt, iron-oxide@Au and Au@Pt, possess very high ORR activity for PEMFCs [14–21].

In this study, a novel Pd_3Fe@Pt/C electrocatalyst with a core–shell structure was prepared via a two-step route. The carbon supported Pd_3Fe alloy is used as a seed for the overgrowth of a Pt shell. The structure of core–shell Pd_3Fe@Pt/C was confirmed by transmission electron microscopy (TEM), X-ray diffraction (XRD) and electrochemical characterization. Intriguingly, it was found that the deposition of platinum on the Pd_3Fe cores exhibits superior ORR activity to that of the Pt/C and Pd_3Fe/C catalysts. These results suggest their use has great potential in PEMFCs as highly efficient and cost-effective catalysts.

* Corresponding author. Tel.: +86 931 7971533; fax: +86 931 7971533.
** Corresponding author. Tel.: +86 931 7970359; fax: +86 931 7970359.
E-mail addresses: wrf38745779@126.com (R. Wang), leizq@nwnu.edu.cn (Z. Lei).

0378-7753/$ – see front matter © 2009 Elsevier B.V. All rights reserved.
doi:10.1016/j.jpowsour.2009.12.015

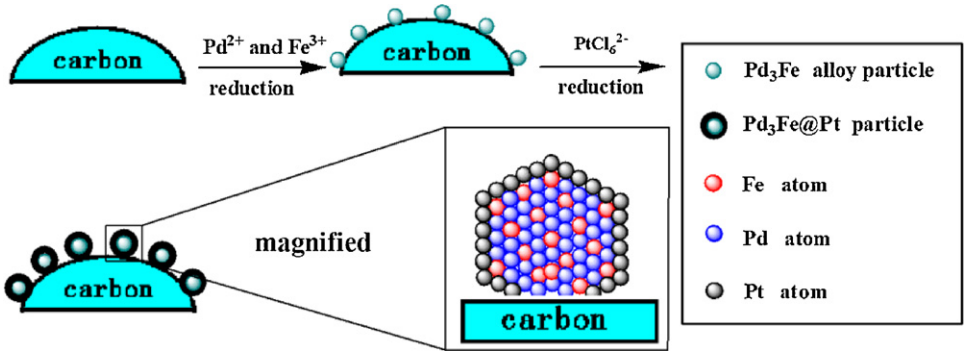

Fig. 1. Illustration of the preparation of the core–shell structured Pd_3Fe@Pt/C catalyst.

2. Experimental

The Pd_3Fe@Pt/C (30 wt% total metal loaded) catalyst with Pt on the surface layers of the Pd_3Fe core was synthesized via a facile, two-step procedure. Firstly, Palladium chloride ($PdCl_2$) was dissolved in a little hydrochloric acid in a flask and 25 mL ethylene glycol (EG) was added as solvent. Following, iron (III) chloride hexahydrate and sodium citrate were added and stirred for 0.5 h. The pH value of the solution was adjusted to ~8 by adding 5 wt% KOH/EG solution. Then, sodium formate and pretreated carbon black (Vulcan XC-72R) were added to the flask with stirring and treated in an ultrasonic bath for 0.5 h, respectively (atom ratio Pd:Fe = 3:1). The resulting solution was transferred into a Teflon-lined autoclave and heated at 180 °C for 6 h. After filtering and washing with ultrapure water, the sample was dried overnight in air at 70 °C. The Pd/C and Pt/C electrocatalysts were prepared by using the same procedure.

Secondly, H_2PtCl_6 (2.5 mg) was dissolved in 20 ml EG in a flask. The pH of the system was adjusted to ~8 by adding 5 wt% KOH/EG solution. Then, the powder of Pd_3Fe/C (50 mg) obtained was added to the flask. The temperature of the resulting mixture was kept at 120 °C for 4 h. Then, the excess of solution was poured out and the product rinsed (8–10 times) with ultrapure water and dried in air at 70 °C. The catalyst obtained is denoted as the Pd_3Fe@Pt/C catalyst.

The particle size and morphology of the catalysts were analyzed by a Tecnai G220S-TWIN (FEI Company) TEM operating at 200 kV. The average chemical composition for Pd_3Fe@Pt/C catalyst was determined using the EDX technique coupled to TEM. XRD patterns were recorded on a Shimadzu XD-3A (Japan) diffractometer, using Cu Ka radiation operated at 35 kV and 40 mA at room temperature.

The electrochemical experiments were performed using an electrochemical work station (CHI604). A conventional three-electrode cell was used, including an Ag/AgCl electrode as the reference electrode, a platinum wire as the counter electrode, and a modified glass carbon electrode (5 mm in diameter) as the working electrode. All potentials presented are quoted with respect to the reversible hydrogen electrode (RHE). The catalyst ink was produced by mixing 5 mg of the catalyst ultrasonically in 1 mL Nafion/ethanol (0.25% Nafion). 8 μL suspensions were then quantitatively transferred to the surface of polished glassy carbon electrode, followed by drying in air at room temperature. Before each measurement, the solution was purged with high-purity N_2 or O_2 gas for at least 30 min to ensure the gas saturated.

3. Results and discussion

In order to develop high active catalysts comparable to the current state-of-art Pt catalysts, a new strategy was developed to prepare Pd_3Fe@Pt/C electrocatalyst with core–shell structure as shown in Fig. 1. It was reported that the loss of surface area is 12.5% due to Pd_3Fe@Pt particles being in contact with the carbon support [22]. We assume that the Pt shell of the 87.5% surface area of Pd_3Fe nanoparticles is Pt atoms covered (shown in Fig. 1), which would be the optimal Pt coverage. Cubic structured Pt acting as seeds for overgrowth of Pd or Au rods and epitaxial growth of Pt on Pd nanoplates have been reported previously [23,24]. In this report, the carbon supported Pd_3Fe@Pt catalyst was synthesized by a two-step reduction process. Firstly, well-defined carbon supported Pd_3Fe alloy nanoparticles were synthesized by an organic colloid method [25]. Secondly, the carbon supported Pd_3Fe alloys act as seeds for overgrowth of the Pt shell. Pt layer was deposited around Pd_3Fe by reducing the H_2PtCl_6 with EG at 120° C.

The reasons why the Pd_3Fe was chosen as core are as follows: firstly, the cost of catalysts could be lowered considerably by using cheap metal Fe to replace some of high cost Pd in the core; secondly, the PdFe alloy nanoparticles which have a very high activity for the ORR have been reported and the optimized ratios of Pd and Fe is 3:1 [26–28]. The Pt shell on the Pd_3Fe nanoparticle has two roles. Firstly, it protects the non-noble core from dissolving in the acidic electrolyte. Secondly, the shell can improve the catalytic properties [29].

The composition of Pd_3Fe@Pt/C electrocatalyst was determined by EDX analysis. The EDX composition of the prepared electrocatalysts is close to the nominal value. However, EDX allows only the estimation of the atomic ratio in the whole catalyst, and no statement can be made about the surface composition.

XRD patterns of Pt/C, Pd/C, Pd_3Fe/C and Pd_3Fe@Pt/C catalysts are shown in Fig. 2. The peak at about $2\theta = 24.8°$ in all samples is associated with the carbon support (2 0 0) diffraction. The XRD profile shows (1 1 1), (2 0 0), (2 2 0) and (3 1 1) diffraction

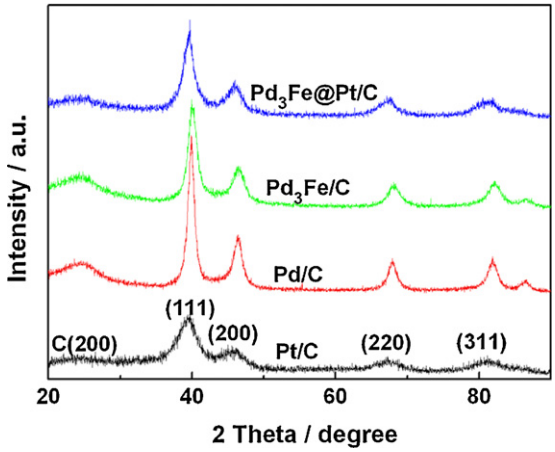

Fig. 2. The XRD patterns of Pt/C, Pd/C, Pd_3Fe/C and Pd_3Fe@Pt/C catalysts.

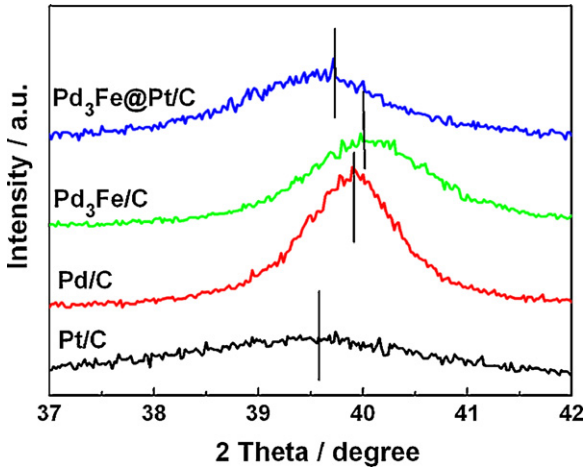

Fig. 3. The enlarged (1 1 1) peaks of the Pt/C, Pd/C, Pd_3Fe/C and Pd_3Fe@Pt/C catalysts.

peaks assigned to the catalyst face-centered cubic (fcc) crystalline structure. Fig. 3 shows the enlarged (1 1 1) peaks of the Pt/C, Pd/C, Pd_3Fe/C and Pd_3Fe@Pt/C catalysts, respectively. Using the Debye–Scherrer equation relating to the (1 1 1) peak broadness, the mean particle size could be evaluated from the literature [30]. The average particle size of the Pt/C, Pd/C and Pd_3Fe/C is 3.9 nm, 5.9 nm and 4.4 nm, respectively. The Pd_3Fe/C shows a pattern with diffraction angles shifting to higher positions compared to Pd/C, which reflect lattice contraction due to the replacement of part of Pd with Fe [26]. As can be seen from Fig. 2, the (1 1 1) peak broadness of Pd_3Fe@Pt/C is relative larger than that of Pd_3Fe/C, suggesting that Pd_3Fe@Pt/C has a composite-phase structure which consists of the Pt as shell and the Pd_3Fe alloy as core. The peak separation results (using Jade software) show that the mean particle size of Pd_3Fe@Pt/C is 4.7 nm, suggesting that the Pt shell is monolayer.

The morphologies of the catalyst nanoparticles were determined using TEM, and the results are presented in Fig. 4. The nanosized particles have predominantly spherical morphology with a uniform distribution on the carbon support. The average particle size of the Pd_3Fe/C and Pd_3Fe@Pt/C catalysts are ca. 4.4 nm and 4.8 nm, respectively. Based on the data of diameter of the catalysts particles and the atomic radius of Pt (http://rsh.nst.pku.edu.cn/element/), the estimated thickness of the Pt shell is about 0.2 nm, i.e., the Pt shell is a monolayer. This result is consistent with the result obtained from XRD data. Despite the small size of the nanoparticles, particle agglomeration is very rare, probably because of the large number of nucleation centers available on the surface of the carbon.

Fig. 5 shows the high resolution TEM (HRTEM) of the Pd_3Fe/C (a) and Pd_3Fe@Pt/C (b) electrocatalysts. In Fig. 5(a) and (b), the continuous ring in the selected area electron diffraction (SAED) pattern (inserted) indicates that the Pd_3Fe/C and Pd_3Fe@Pt/C nanoparticles are polycrystalline. According to the HRTEM image and SAED, the distance between two adjacent lattice planes (indicated by the d spacer in the image) is approximately 0.2285 nm and 0.2353 nm for Pd_3Fe/C and Pd_3Fe@Pt/C, respectively. The calculated (1 1 1) plane distance of the Pd_3Fe core and Pt shell (see Fig. 5) is similar to the results in literature [8,31]. The HRTEM results also suggest that reduced Pt is formed as a shell covering the Pd_3Fe core. The reason why the Pt is reduced and then covers the Pd_3Fe particles can be attributed to: (i) the interaction between the metals is stronger than that between metal and carbon; (ii) platinum crystallite and Pd_3Fe alloy are all with fcc structure, which favors the epitaxial growth of the Pt shell on the Pd_3Fe core. This unique core–shell structure can improve the performance of the ORR, which is discussed as follows.

The electrochemical properties of materials are very sensitive to their surface composition and structure. Therefore, the presence of a shell over nanosized particles, which is difficult to detect by most physical characterization methods, could be manifested by the electrochemical responses of core–shell particles [32]. Fig. 6 shows the representative cyclic voltammetric curves in N_2-purged 0.5 M H_2SO_4 electrolyte, recorded on Pt/C, Pd/C, Pd_3Fe/C and Pd_3Fe@Pt/C catalysts from 0 V to 1.2 V (RHE). The potential interval between 0 V to 0.2 V shows the electrochemical fingerprint. The current densities in the hydrogen adsorption/desorption and oxide formation/reduction of Pd_3Fe/C are lager than those of Pd/C. The results are similar to the results in the literature [33]. The cathode peak at 0.65 V (RHE) is attributed to the reduction of the Pd oxide produced [34]. It is interesting that the peak of the reduction potential of Pd_3Fe@Pt/C catalyst is more positive than that of Pd/C and Pd_3Fe/C catalysts, which indicates that the Pd_3Fe surface has already been covered with a Pt shell.

Normally, the electrochemical surface area (ECSA) of Pt-based catalysts under the hydrogen adsorption/desorption peak can be estimated from the integrated charge of the hydrogen absorption region of the CV. The ECSA of different catalysts were calculated according to methods in the literature [35,36]. The ECSA are 86.11 $m^2\,g^{-1}$ metals for Pt/C and 63.49 $m^2\,g^{-1}$ metals for Pd_3Fe@Pt/C. Based on the Pt mass, the specific ECSA of Pd_3Fe@Pt/C is 186.74 $m^2\,g^{-1}$ Pt, which is 2.18 times larger than that of Pt/C

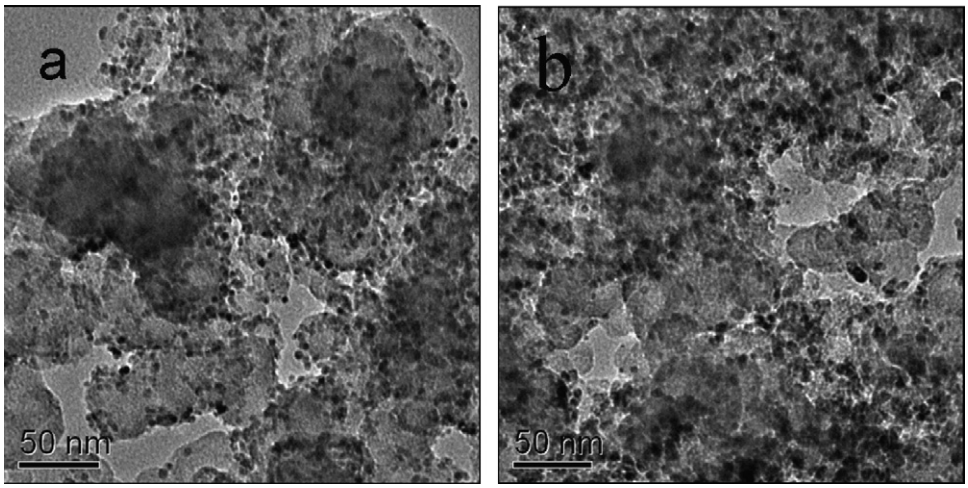

Fig. 4. TEM images of prepared Pd_3Fe/C (a) and Pd_3Fe@Pt/C (b) electrocatalysts.

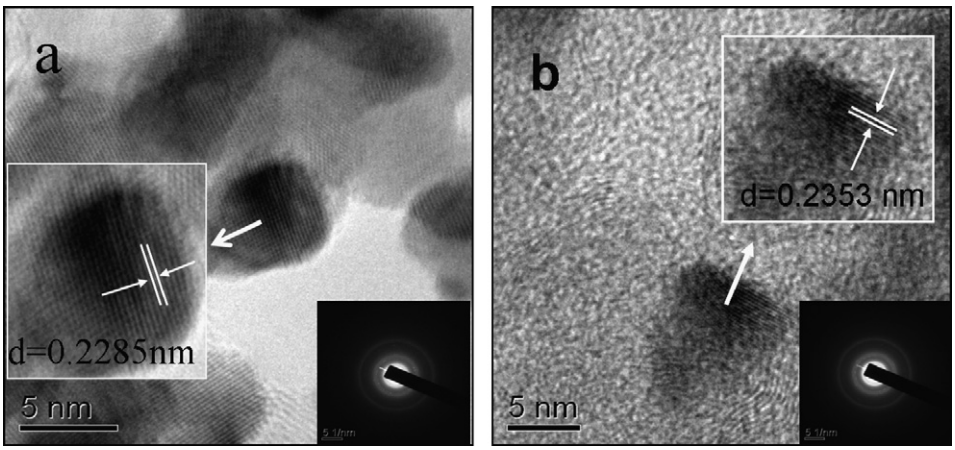

Fig. 5. High resolution TEM images of the Pd_3Fe/C (a) and $Pd_3Fe@Pt/C$ (b) electrocatalysts. Insert shows the corresponding selected area electron diffraction.

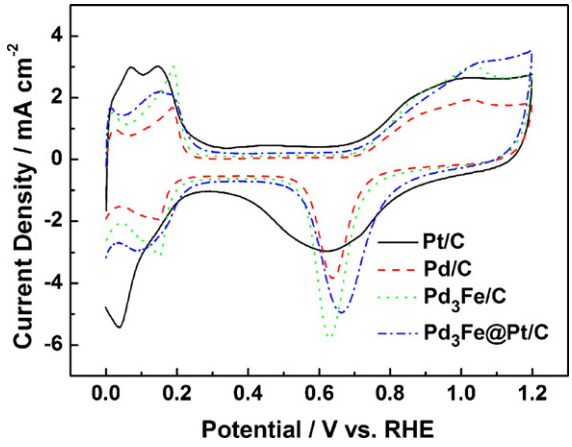

Fig. 6. Cyclic voltammograms of Pt/C, Pd/C, Pd_3Fe/C and $Pd_3Fe@Pt/C$ catalysts in 0.5 M H_2SO_4 solution under N_2 atmosphere. Scan rate: 50 mV s^{-1}. Rotation speed: 300 rpm.

catalyst. It suggests that the $Pd_3Fe@Pt/C$ catalyst show higher utilization of Pt than those of Pt/C. The higher surface area results in a higher catalytic activity [1]. These results suggest that a simple route to the enhancement of catalytic efficiency is to modify the morphology using a Pt layer.

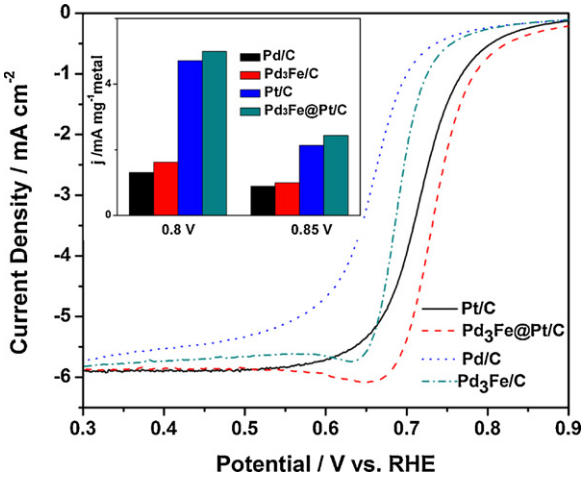

Fig. 7. Polarization curves for ORR on Pd/C, Pd_3Fe/C, Pt/C and $Pd_3Fe@Pt/C$ in an O_2-saturated 0.5 M H_2SO_4 solution at room temperature. Inserted figure shows the mass specific activity for Pd/C, Pd_3Fe/C, Pt/C and $Pd_3Fe@Pt/C$ at 0.8 V and 0.85 V, respectively. Scan rate: 5 mV s^{-1}. Rotation speed: 1600 rpm.

The ORR on noble metal surface is one of the most widely studied reactions in electrochemistry [37]. Herein we focus on their performance in ORR in terms of their potential utilization as cathode catalysts in PEMFCs. Fig. 7 displays the ORR polarization curve for $Pd_3Fe@Pt/C$ in O_2-saturated 0.5 M H_2SO_4 solution at room tempera-

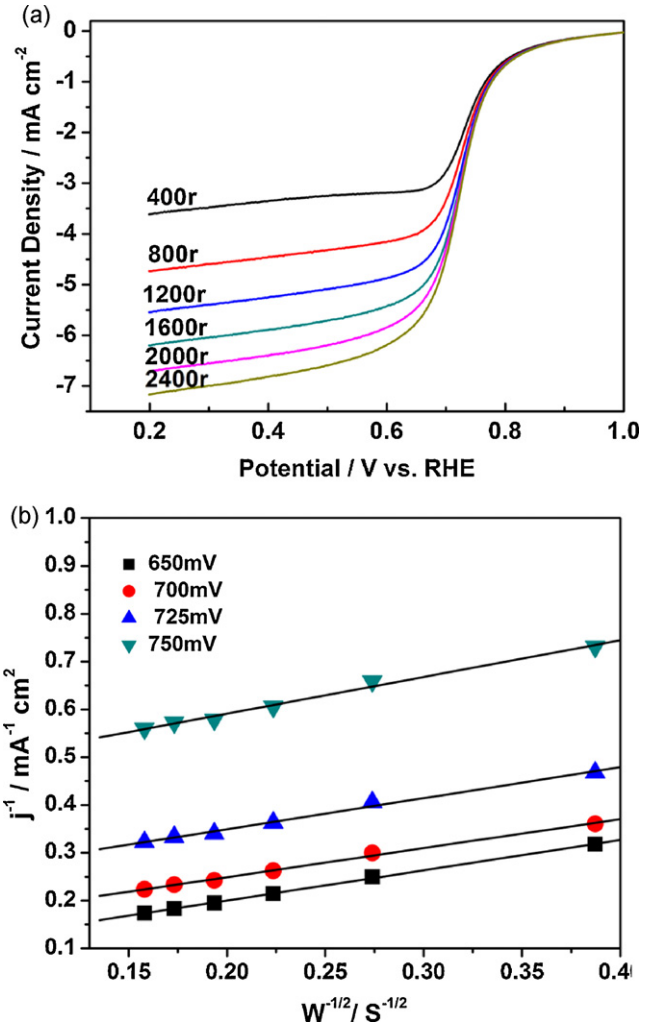

Fig. 8. (a) Polarization curves for ORR on $Pd_3Fe@Pt/C$ in an O_2-saturated 0.5 M H_2SO_4 solution at different rotation rates. (b) The corresponding Koutecky–Levich plots at different potentials. Scan rate: 5 mV s^{-1}.

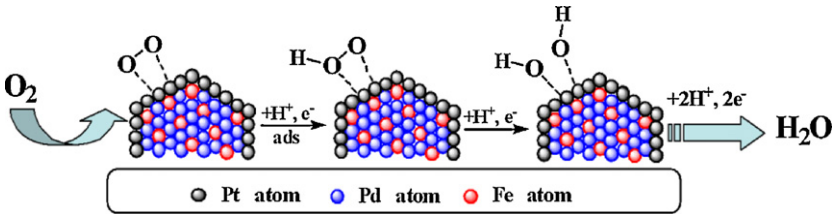

Fig. 9. The mechanism of reduction of O_2 on the Pd_3Fe@Pt/C electrocatalyst.

ture with sweep rate of 5 mV s^{-1} and a rotation rate of 1600 rpm. For comparison, Pd/C, Pd_3Fe/C and Pt/C catalysts are also shown in this figure. It is clear that the activity of Pd is greatly enhanced by alloying with Fe, which is consistent with the results in the literature [8]. It is found that the curve obtained in the case of the Pd_3Fe@Pt/C catalyst shifts to a more positive value than that of the others at onset potential. Intriguingly, the half-wave potential of the Pd_3Fe@Pt/C catalyst is 739 mV, which is a shift of 21 mV more positive to that of the Pt/C (718 mV) catalyst. For the Pd_3Fe@Pt/C catalyst, the diffusion-limiting current were obtained in the potential region of about 0.65 V, whereas a mixed kinetic-diffusion control region occurs between 0.7 V and 0.8 V. The kinetic current was calculated from the ORR polarization curve by mass-transport correction and normalized to the mass activity of the different catalysts. As shown in the insert of Fig. 7, the Pd_3Fe@Pt/C exhibits a mass specific activity of 5.00 mA mg^{-1} metal at 0.8 V and 2.41 mA mg^{-1} metal at 0.85 V (RHE), respectively. It shows that the activity of the Pd_3Fe@Pt/C for ORR is much higher than that of Pd_3Fe/C, and also higher than that of Pt/C. Furthermore, the total mass specific activity (taking into account all the metal in the catalyst, i.e., Pt, Pd and Fe) of the core–shell structured Pd_3Fe@Pt/C is still highest among all the tested catalysts. Considering that only surface atoms can catalyze the reaction, the results can be explained by the facts that atoms of Pt form a shell on the Pd_3Fe core and a synergetic effect between the Pd_3Fe core and the Pt shell.

Fig. 8(a) shows a set of polarization curves for ORR on Pd_3Fe@Pt/C in an O_2-saturated 0.5 M H_2SO_4 solution. The main characteristic of these polarization curves (shown in Fig. 8(a)) is the defined charge transfer control, mixed and mass transfer region. It is obviously that the current densities are roughly dependent on $\omega^{1/2}$. The corresponding Koutecky–Levìch plots result in parallel straight lines as shown in Fig. 8(b). The good linearity and parallelism of the plots indicate first order kinetics with respect to molecular oxygen [38]. The kinetic current density is proportional to the intrinsic activity of the catalyst. The analysis of the catalytic currents as a function of the rotation rate using the Koutecky–Levìch equation from the literature is shown below [39].

$$I^{-1} = I_k{}^{-1} + I_d{}^{-1} = I_k{}^{-1} + (B\omega^{1/2})^{-1}$$
$$= (nFkC_{O_2})^{-1} + (0.62nFAC_{O_2}D_{O_2}{}^{2/3}\nu^{-1/6}\omega^{1/2})^{-1} \quad (1)$$

where I is the observed experimentally current, I_k is the kinetic current, I_d is the diffusion limited current, k is the reaction rate constant, n is the number of electrons exchanged per O_2 molecule, F is the Faraday constant (96,485 C mol^{-1}), A is the geometric area of the glassy carbon electrode, C_{O_2} is the bulk oxygen concentration (1.1×10^{-3} mol L^{-1}), D_{O_2} is the diffusion coefficient of molecular oxygen (1.4×10^{-5} mol s^{-1}), ν is the cinematic viscosity of the electrolyte (0.01 cm^2 s^{-1}) and ω is the electrode rotation speed. The B parameter is defined as

$$B = 0.62nFAC_{O_2}D_{O_2}{}^{2/3}\nu^{-1/6} \quad (2)$$

According to Eq. (2), the corresponding B value is calculated in agreement with the theoretical value calculated for a four-electron process. It is clear that the ORR on Pd_3Fe@Pt/C catalyst at different potentials follows the same 4-electron reaction pathway as that on Pt [40].

The mechanism of the ORR is still under discussion in the literature [41]. Density functional theory was employed to investigate the thermodynamics of key steps of the electrocatalytic ORR in many cases. It was found that Pt is the most effective single metal catalyst for ORR [42]. We propose a four-electron reaction pathway (shown in Fig. 9) of the ORR for the synthesized Pd_3Fe@Pt/C catalyst, which is able to explain our experimental results. Firstly, an oxygen molecule occupies two Pt sites by side-on adsorption. As oxygen is strongly electronegative, it will take up electrons from the catalyst. The uptake of a proton to form the adsorbed species HO_{ad} is the next step. In the last step the adsorbed HO_{ad} is reduced to water as in the literature [43]. All the alloy catalysts tested were covered with layer of Pt, in which the distance of Pt–Pt on the layer of Pt may be similar to that of pure Pt [44]. For that reason, the ORR on Pd_3Fe@Pt/C catalyst could go through the same 4-electron reaction pathway as that on Pt. An enhanced electrocatalytic performance on Pd_3Fe@Pt/C catalyst may result from electronic modification of the Pt layer. It probably enhances not only the overall ORR rate but also the possibility of end-on type O_2 adsorption due to increase in the coverage and bond strength [45].

4. Conclusion

In summary, a facile and effective way to prepare core–shell Pd_3Fe@Pt/C catalyst under mild reaction conditions has been developed. The Pd_3Fe@Pt/C catalyst has a higher surface area and exhibits an enhanced electrocatalytic performance, which is evident from the observed cyclic voltammetric curves and ORR as compared with those of the Pd_3Fe/C and Pt/C catalysts. The Koutecky–Levìch plots indicate that the ORR, which catalyzed by the Pd_3Fe@Pt/C, could go through a four-electron pathway similar to that of the ORR on the Pt. The high activity of the Pd_3Fe@Pt/C catalyst for the ORR suggests that the synthesized catalyst could be an economically viable candidate to replace pure Pt catalysts as an ultralow-Pt cathode catalyst in PEMFCs. Future work on the ORR catalytic stability of this catalyst will be carried out in the near future.

Acknowledgment

We would like to thank the Key Project of Ministry of Education Foundation (209129) for financially supporting this work.

References

[1] H.P. Liang, H.M. Zhang, J.S. Hu, Y.G. Guo, L.J. Wan, C.L. Bai, Angew. Chem. Int. Ed. 43 (2004) 1540–1543.
[2] G. Zehl, G. Schmithals, A. Hoell, S. Haas, C. Hartnig, I. Dorbandt, P. Bogdanoff, S. Fiechter, Angew. Chem. Int. Ed. 46 (2007) 7311–7314.
[3] A. Serovl, C. Kwak, Appl. Catal. B: Environ. 90 (2009) 313–320.
[4] Y. Kawasoe, S. Tanaka, T. Kuroki, H. Kusaba, K. Ito, Y. Teraoka, K. Sasaki, J. Electrochem. Soc. 154 (2007) B969–B975.
[5] H. Yang, N. Alonso-Vante, C. Lamy, D.L. Akins, J. Electrochem. Soc. 152 (2005) A704–A709.
[6] B. Lim, M. Jiang, P.H.C. Camargo, E.C. Cho, J. Tao, X. Lu, Y. Zhu, Y. Xia, Science 324 (2009) 1302–1305.

[7] Q. Huang, H. Yang, Y. Tang, T. Lu, D.L. Akins, Electrochem. Commun. 8 (2006) 1220–1224.
[8] M. Shao, P. Liu, J. Zhang, R. Adzic, J. Phys. Chem. B 111 (2007) 6772–6775.
[9] K. Persson, A. Ersson, N. Iverlund, S. Jaras, J. Catal. 231 (2005) 139–150.
[10] H.A. Gasteiger, N.M. Markovic, Science 324 (2009) 48–49.
[11] K.J.J. Mayrhofer, V. Juhart, K. Hartl, M. Hanzlik, M. Arenz, Angew. Chem. Int. Ed. 48 (2009) 3529–3531.
[12] J. Luo, L. Wang, D. Mott, P.N. Njoki, Y. Lin, T. He, Z. Xu, B.N. Wanjana, I.I.S. Lim, C.J. Zhong, Adv. Mater. 20 (2008) 4342–4347.
[13] M. Shao, K. Sasaki, N.S. Marinkovic, L. Zhang, R.R. Adzic, Electrochem. Commun. 9 (2007) 2848–2853.
[14] K. Shimizu, I.F. Cheng, C.M. Wai, Electrochem. Commun. 11 (2009) 691–694.
[15] M.H. Lee, J.S. Do, J. Power Sources 188 (2009) 353–358.
[16] J.S. Do, Y.T. Chen, M.H. Lee, J. Power Sources 172 (2007) 623–632.
[17] Z.D. Wei, Y.C. Feng, L. Li, M.J. Liao, Y. Fu, C.X. Sun, Z.G. Shao, P.K. Shen, J. Power Sources 180 (2008) 84–91.
[18] L. Wang, J. Luo, Q. Fan, M. Suzuki, I.S. Suzuki, M.H. Engelhard, Y. Lin, N. Kim, J.Q. Wang, C.J. Zhong, J. Phys. Chem. B 109 (2005) 21593–21601.
[19] L. Wang, J. Luo, M.M. Maye, Q. Fan, Q. Rendeng, M.H. Engelhard, C. Wang, Y. Lin, C.J. Zhong, J. Mater. Chem. 15 (2005) 1821–1832.
[20] H.Y. Park, M.J. Schadt, L. Wang, I.I.S. Lim, P.N. Njoki, S.H. Kim, M.Y. Jiang, J. Luo, C.J. Zhong, Langmuir 23 (2007) 9050–9056.
[21] N. Kristian, X. Wang, Electrochem. Commun. 10 (2008) 12–15.
[22] J. Yang, J.Y. Lee, Q. Zhang, W. Zhou, Z.J. Liu, J. Electrochem. Soc. 155 (2008) B776–B781.
[23] H. Lee, S.E. Habas, G.A. Somorjai, P.J. Yang, J. Am. Chem. Soc. 130 (2008) 5406–5407.
[24] B. Lim, J. Wang, P.H.C. Camargo, M. Jiang, M.J. Kim, Y. Xia, Nano Lett. 8 (2008) 2535–2540.
[25] R. Wang, S. Liao, S. Ji, J. Power Source 180 (2008) 205–208.
[26] M.H. Shao, K. Sasaki, R.R. Adzic, J. Am. Chem Soc. 128 (2006) 3526–3527.
[27] W. Li, P. Haldar, Electrochem. Commun. 11 (2009) 1195–1198.
[28] S. Songa, Y. Wang, P. Tsiakaras, P.K. Shen, Appl. Catal. B: Environ. 78 (2008) 381–387.
[29] J. Zhang, F.H.B. Lima, M.H. Shao, K. Sasaki, J.X. Wang, J. Hanson, R.R. Adzic, J. Phys. Chem. B 109 (2005) 22701–22704.
[30] V.I. Zaikovskii, K.S. Nagabhushana, V.V. Kriventsov, K.N. Loponov, S.V. Cherepanova, R.I. Kvon, H. Bönnemann, D.I. Kochubey, E.R. Savinova, J. Phys. Chem. B 110 (2006) 6881–6890.
[31] B. Lim, X. Lu, M. Jiang, P.H. Camargo, C.E.C. Cho, E.P. Lee, Y. Xia, Nano Lett. 8 (2008) 4043–4047.
[32] Y. Chen, F. Yang, Y. Dai, W. Wang, S. Chen, J. Phys. Chem. C 112 (2008) 1645–1649.
[33] Y. Gochi-Ponce, G. Alonso-Nunez, N. Alonso-Vante, Electrochem. Commun. 8 (2006) 1487–1491.
[34] G. Ramos-Sanchez, H. Yee-Madeira, O. Solorza-Feria, Int. J. Hydrogen Energy 33 (2008) 3596–3600.
[35] X. Li, W.X. Chen, J. Zhao, W. Xing, Z.D. Xu, Carbon 43 (2005) 2168–2174.
[36] M.H. Shao, K. Sasaki, R.R. Adzic, J. Am. Chem. Soc. 128 (2006) 3526–3527.
[37] R. Srivastava, P. Mani, N. Hahn, P. Strasser, Angew. Chem. Int. Ed. 46 (2007) 8988–8991.
[38] C. Xu, Y. Zhang, L. Wang, L. Xu, X. Bian, H. Ma, Y. Ding, Chem. Mater. 21 (2009) 3110–3116.
[39] R.H. Castellanos, A.L. Ocampo, J. Moreira, P. Sebastian, Int. J. Hydrogen Energy 26 (2001) 1301–1306.
[40] V. Stamenkovic, T.J. Schmidt, P.N. Ross, N.M. Markovic, J. Phys. Chem. B 106 (2002) 11970–11979.
[41] N.M. Marcovic, P.N. Ross, Surf. Sci. Rep. 45 (2002) 117–229.
[42] Y. Wang, P.B. Balbuena, J. Phys. Chem. B 109 (2005) 18902–18906.
[43] H. Kuhn, A. Wokaun, G.G. Scherer, Electrochim. Acta 52 (2007) 2322–2327.
[44] T. Toda, H. Igarashi, H. Uchida, M. Watanabe, J. Electrochem. Soc. 146 (1999) 3750–3756.
[45] N. Wakabayashi, M. Takeichi, H. Uchida, M. Watanabe, J. Phys. Chem. B 109 (2005) 5836–5841.